Journal of Reproduction and Development, Vol. 64, No 1, 2018

—Original Article—

Mancozeb impairs the ultrastructure of mouse granulosa cells in a dose-dependent manner

Maria Grazia PALMERINI[1)], Manuel BELLI[1)], Stefania Annarita NOTTOLA[2)], Selenia MIGLIETTA[2)], Serena BIANCHI[1)], Sara BERNARDI[1)], Sevastiani ANTONOULI[1)], Sandra CECCONI[1)], Giuseppe FAMILIARI[2)] and Guido MACCHIARELLI[1)]

[1)]*Department of Life, Health and Environmental Sciences, University of L'Aquila, 67100 L'Aquila, Italy*
[2)]*Deparment of Anatomy, Histology, Forensic Medicine and Orthopaedics, La Sapienza University of Rome, 00161 Rome, Italy*

Abstract. Mancozeb, an ethylene bis-dithiocarbamate, is widely used as a fungicide and exerts reproductive toxicity *in vivo* and *in vitro* in mouse oocytes by altering spindle morphology and impairing the ability to fertilize. Mancozeb also induces a premalignant status in mouse granulosa cells (GCs) cultured *in vitro*, as indicated by decreased p53 expression and tenuous oxidative stress. However, the presence and extent of ultrastructural alterations induced by mancozeb on GCs *in vitro* have not yet been reported. Using an *in vitro* model of reproductive toxicity, comprising parietal GCs from mouse antral follicles cultured with increasing concentrations of mancozeb (0.001–1 μg/ml), we sought to ascertain the *in vitro* ultrastructural cell toxicity by means of transmission (TEM) and scanning (SEM) electron microscopy. The results showed a dose-dependent toxicity of mancozeb on mouse GCs. Ultrastructural data showed intercellular contact alterations, nuclear membrane irregularities, and chromatin marginalization at lower concentrations, and showed chromatin condensation, membrane blebbing, and cytoplasmic vacuolization at higher concentrations. Morphometric analysis evidenced a reduction of mitochondrial length in GCs exposed to mancozeb 0.01−1 μg/ml and a dose-dependent increase of vacuole dimension. In conclusion, mancozeb induced dose-dependent toxicity against GCs *in vitro*, including ultrastructural signs of cell degeneration compatible with apoptosis, likely due to the toxic breakdown product ethylenethiourea. These alterations may represent a major cause of reduced/delayed/missed oocyte maturation in cases of infertility associated with exposure to pesticides.

Keywords: Granulosa cells, Mancozeb, Scanning electron microscopy, Transmission electron microscopy, Ultrastructure

(**J. Reprod. Dev. 64:** 75–82, 2018)

Mancozeb, an ethylene bis-dithiocarbamate (manganese/zinc ethylene bis-dithiocarbamate), is widely used as a broad-spectrum organometallic fungicide for field crops, fruits, nuts, vegetables, and ornamental plants. Introduced in 1962, mancozeb continues to play a significant role in the global fungicide market, mostly because of its low acute toxicity and long persistence on leaves. The toxicity of mancozeb is related to metabolic processes, which generate ethylenethiourea, and to its subsequent bioaccumulation in tissues and biological fluids, even at very low concentrations [1].

The toxic effects associated with the routine use of mancozeb have been studied *in vivo* and *in vitro* in various animal models and in humans (see for review [2–4]). Available data have provided evidence of the endocrine-disrupting activity of this pesticide, including impairment of the hypothalamic-pituitary-gonadal axis [5, 6]. Animal studies have provided high-to-moderate confidence of reproductive and developmental toxicity for mancozeb, while human observational studies have indicated a moderate-to-low level of confidence [2]. Risk assessment procedures should also consider adverse cumulative effects associated with the use of mixtures of pesticides, including mancozeb, responsible for persistent developmental and reproductive toxicity [7, 8].

Data from *in vitro* experiments have revealed dose-dependent alteration of the spindle in mouse oocyte-cumulus complexes (OCCs) exposed to increasing concentrations of the fungicide (0.001, 0.01, 0.1, and 1 μg/ml) [9]. Although 98% of control oocytes showed normally assembled spindles, located at the periphery of the cell and with well-aligned chromosomes on the metaphase plate, mancozeb induced a significant increase in abnormal spindle configurations. The fungicide induced microtubule elongation and spindle length reduction, especially at the highest concentrations (0.1 and 1 μg/ml) [9]. Cytoskeletal alterations were also found in mouse granulosa cells (GCs) exposed to increasing concentrations of mancozeb. After 24 h of *in vitro* culture (IVC), cell reshaping and changes in the actin cortical cytoskeleton, evaluated by immunofluorescence, were visible with 0.1 and 1 μg/ml concentrations. A marked rearrangement in stress fibers was also detected following prolonged culture (36 h), even under exposure to 0.01 μg/ml of mancozeb [10]. A similar pattern of cytoskeletal alterations was observed in human GCs exposed to concentrations higher than 0.01 μg/ml for 36 h. These changes were accompanied by dose- and time-dependent modifications in GC

Received: October 30, 2017
Accepted: November 21, 2017
Published online in J-STAGE: December 11, 2017

Correspondence: MG Palmerini (e-mail: mariagrazia.palmerini@univaq.it)

morphology, which changed from an epithelial-like to a spindle-like/elongated shape. Furthermore, mancozeb treatment of both mouse and human GCs led to a marked decrease in p53 mRNA and protein levels, which was likely connected to the observed cell reshaping [10].

Mancozeb targets the mitochondria, as shown by ΔΨm impairment with a subsequent increase in ROS generation, alterations in the cellular redox state, and decreased ATP levels in mouse GCs, detected using cytofluorimetric assays [11]. Interestingly, at the concentration tested (0.01 μg/ml), these alterations were not related to the initiation of apoptosis or DNA damage response but to AKT activation and the maintenance of energy homeostasis [11].

We therefore aimed to ascertain whether the biomolecular alterations and cell reshaping observed following mancozeb exposure were connected to ultrastructural damages and cell-to-cell uncoupling, with subsequent isolation and cell death. We used a model of reproductive toxicity previously described in a study of the hexachlorocyclohexane lindane [12], comprising mouse GCs cultured *in vitro* in the presence or absence of increasing concentrations of mancozeb. Ultrastructural analysis of GCs was performed by transmission (TEM) and scanning (SEM) electron microscopy. Morphometric evaluation of cytoplasmic organelles was also performed.

Materials and Methods

Chemicals

All materials were purchased from Sigma Chemical (St. Louis, MO, USA), unless stated otherwise.

Animals

Swiss CD1 mice (Harlan Italy, Udine, Italy) were housed in individual cages with a 12:12 h light:dark cycle, controlled temperature (21 ± 1°C), and free access to food and water. Prepubertal females (21–23 days old) were intraperitoneally administered 5 IU of PMSG (pregnant mare serum gonadotropin) (Intervet, Milan, Italy) and euthanized 48 h later. Animals were maintained in accordance with the Italian Department of Health Guide for Care and Use of Laboratory Animals. The local committee on animal care and use approved the experimental protocols (Univaq 2012-2015) [10, 11], which were also compliant with international standards of animal care and veterinary medical practice.

GC isolation and experimental protocol

Mouse ovaries were collected, washed in PBS (phosphate buffered saline, pH = 7–7.4) at 37°C, and transferred to culture dishes (Becton Dickinson and Company, Franklin Lakes, NJ, USA) containing MEM Hepes (Life Technologies Italy, Monza MB, Italy). The ovaries were punctured with insulin syringe needles to release the mural GCs. GCs were then transferred into culture dishes for IVC. To assess the reproductive toxicity of mancozeb, GCs were exposed or not (control) to increasing concentrations (0.001, 0.01, 0.1, and 1 μg/ml), as previously reported [10, 12].

In vitro maturation of mouse granulosa cells

GCs were cultured in DMEM (Dulbecco's modified Eagle's medium, GE Healthcare, Little Chalfont, Buckinghamshire, UK) containing 5% FBS (fetal bovine serum) supplemented with 2 mM L-glutamine and antibiotics (100 mM penicillin and 100 μg/ml streptomycin) in 35-mm tissue culture-treated culture dishes for 12 h to allow adhesion [10, 12]. Mancozeb (PESTANAL®, 45553) was dissolved in DMEM to obtain the desired concentrations. GCs were, then, cultured *in vitro* with fresh medium containing or not (Control) increasing concentrations of mancozeb at 37°C and 5% CO_2 for 36 h.

Light microscopy (LM) and transmission electron microscopy (TEM)

Following IVC, GCs were aspirated, gently washed in PBS, centrifuged at 290 rcf (1200 rpm) for 5 min at 37°C, and immediately fixed in 2.5% glutaraldehyde (Agar Scientific, Cambridge Road Stansted Essex, UK)/PBS. The pellets were maintained at 4°C for 2–5 days until the next preparative for TEM [13–18]. Briefly, GCs were embedded in small blocks of 1% agar of about 5 × 5 × 1 mm in size, dehydrated in an ascending series of ethanol, immersed in propylene oxide for solvent substitution, embedded in epoxy resin EMbed-812 (Electron Microscopy Sciences, 1560 Industry Road, Hatfield, PA, USA), and sectioned using a Reichert-Jung Ultracut E ultramicrotome (Reichert Technologies, Munich, Germany). Semi-thin sections (1 mm thick) were stained with Toluidine Blue, examined by LM (Zeiss Axioskop), and photographed using a digital camera (Leica DFC230). Ultra-thin sections (60–80 nm) were cut with a diamond knife, mounted on copper grids, and contrasted with saturated uranyl acetate and lead citrate (SIC, Rome, Italy) before being examined and photographed using Zeiss EM10 and Philips TEM CM100 electron microscopes operating at 80 KV.

The following parameters were evaluated by LM and TEM and used in the qualitative assessment of GCs: general features; cell membrane integrity; type and quality of organelles and inclusions; characteristics of the nucleus, chromatin, and nuclear envelope; and presence and extent of cytoplasmic vacuolization, intercellular projections, blebbing, and cellular debris [19, 20].

Scanning electron microscopy

For SEM observations, IVC was performed on 18-mm sterile polylisinated coverslips placed in culture dishes. Next, adherent GCs were washed in PBS, fixed in 2.5% glutaraldehyde/PBS at 4°C for at least 48 h, and then subjected to SEM specimen preparation [21–26]. Briefly, fixed GCs were post-fixed with osmium tetroxide, washed in PBS, and dehydrated with increasing concentrations of alcohol. Samples were then subjected to critical point drying, mounted onto aluminum stubs, and sputtered with platinum or gold particles before being observed with a scanning electron microscope (Philips XL – 30 CP) under low voltage (3–10 kV).

Morphometric analysis

ImageJ software (http://rsbweb.nih.gov/ij/) was used to measure the number and dimensions of mitochondria and vacuoles observed on low-magnification TEM micrographs of control and mancozeb-treated GCs. For each experimental group, at least 15 GCs from three different experiments were selected for morphometric analysis.

Statistical analysis

All data are expressed as means ± standard deviation (SD). Statistical comparisons were performed using one-way ANOVA

with Tukey's honest significant difference (HSD) tests for post-hoc analysis (GraphPad InStat. GraphPad Software, La Jolla, USA). Differences in values were considered significant if $P < 0.05$.

Results

Control

Under LM, GCs showed a round-to-ovoid shape with a high nucleus:cytoplasm ratio. Nuclei, delimited by an intensely stained nuclear membrane, presented a variable number of nucleoli (Fig. 1A, inset). TEM of GCs showed that nuclei were delimited by a roundish, continuous, and electron-dense nuclear membrane (Fig. 1A). Chromatin was uniformly distributed or sometimes clustered in central clumps. In the cytoplasm, numerous groups of round/elongated mitochondria and tubular elements of the smooth endoplasmic reticulum (SER) were observed (Fig. 1A, 1B). Vesicles of the Golgi apparatus and lipid droplets, which are highly electron-dense, were occasionally found. Secondary lysosomes were also occasionally found (Fig. 1B). The plasma membrane presented numerous microvilli and cytoplasmic projections (not shown).

SEM showed GC stratification on the culture support, with a first layer of irregular and flattened cells and outer layers comprising rounder cells (Fig. 1C). The GC surface was densely covered with microvilli, even if adherent GCs, with a reduced length and distribution of microvilli and pseudopodia, were occasionally found. Numerous long and thin cytoplasmic protrusions (pseudopodia) connected adjacent GCs (Fig. 1C). The main results are summarized in Table 1.

Mancozeb 0.001 μg/ml

GCs cultured *in vitro* with the lowest concentration of mancozeb (0.001 μg/ml) presented morphological features similar to the controls under LM (Fig. 1D, inset).

Under TEM, GCs showed a round-to-ovoid shape with large roundish nuclei, delimited by an intact electron-dense nuclear membrane (Fig. 1D). Chromatin distribution did not differ from that of controls, with spots of heterochromatin normally located in the center of the cell or more rarely eccentric. The GC cytoplasm showed numerous round/ovoid mitochondria delimited by a double electron-dense mitochondrial membrane, with numerous intensely stained mitochondrial cristae (Fig. 1E). Lipid droplets and tubular elements of the endoplasmic reticulum (ER) were also found. Numerous intercellular contacts were observed to have been established by intercellular junctions and projections (Fig. 1D).

SEM analysis showed that the distribution of GCs and surface morphology were similar to those of controls. A retraction of intercellular connections and reduction in length and number of microvilli was occasionally observed. Cytoplasmic blebs were also occasionally found (Fig. 1F). The main results are summarized in Table 1.

Mancozeb 0.01 μg/ml

GCs cultured in the presence of 0.01 μg/ml mancozeb occasionally showed smaller cells among normal-sized elements, and intensely stained intracellular spots (Fig. 2A, inset).

TEM showed the presence of alterations such as chromatin marginalization, nuclear membrane invaginations, vacuolization, and membrane blebbing (Fig. 2A). No alterations were observed in organelles such as mitochondria, ER, and lipid droplets.

SEM showed smooth GCs with short microvilli and occasional blebbing (Fig. 2B), and cytoplasmic projections were reduced in number and length (Fig. 2B). The main results are summarized in Table 1.

Mancozeb 0.1 μg/ml

Cells cultured in the presence of mancozeb 0.1 μg/ml showed an irregular shape under LM, as well as varying dimensions and the occasional presence of dark cytoplasmic bodies (Fig. 2C, upper inset).

Under TEM, GCs did not show evident alterations in mitochondria, lipid droplets, and ER compared with previous groups (Fig. 2C). However, a pattern of alterations to the nucleus was frequently observed, as well as nuclear membrane invagination, chromatin condensation, and marginalization. An evident increase in vacuolization and blebbing, as well as a reduction in intercellular contacts, was also noticed. Degenerating GCs, characterized by cytoplasmic fragments often in proximity to integral nuclei or organelles, were frequently observed (lower inset of Fig. 2C).

By SEM, the presence of blebbing (Fig. 2D, inset), the retraction of intercellular communications, and a diminution of microvilli was frequently found (Fig. 2D). The main results are summarized in Table 1.

Mancozeb 1 μg/ml

At the highest concentration tested, large vacuoles were frequently observed in the cytoplasm of GCs, and numerous cell fragments were dispersed among the cells, as seen under LM (Fig. 2E, inset).

Ultrastructural TEM analysis showed the increased presence of peculiar alterations to the nucleus, as observed in the previous group (0.1 μg/ml) but more frequent, and/or to the cytoplasm, such as vacuolization and membrane blebbing (Fig. 2E). Mitochondrial cristae appeared less electron-dense. Degenerating cells, recognizable by the presence of membrane-bound cell fragments dispersed in cell debris, were commonly observed (Fig. 2E).

Under SEM, numerous blebs were observed on the surface of GCs, often characterized by a smooth appearance with rare short microvilli (Fig. 2F, inset). A reduction in pseudopodia and retraction of intercellular contacts was also observed (Fig. 2F). The main results are summarized in Table 1.

Morphometric analysis

Mitochondrial length did not differ between the control and mancozeb 0.001 μg/ml groups (0.550 ± 0.074 μm *vs*. 0.539 ± 0.127 μm, respectively; $P > 0.05$). However, a significant reduction in mitochondrial length was observed in GCs exposed to 0.01 μg/ml (0.364 ± 0.091 μm), 0.1 μg/ml (0.366 ± 0.074 μm), and 1 μg/ml (0.437 ± 0.087 μm) mancozeb compared to that of control and mancozeb 0.001 μg/ml groups ($P < 0.01$) (Table 2). The mean mitochondrial count was significantly increased only in GCs exposed to mancozeb 0.1 μg/ml (40 ± 6) compared to that of the other groups (approximately 25) ($P < 0.05$).

Vacuole length increased significantly in a dose-dependent manner, ranging from 0.336 ± 0.141 μm in the control group to 1.059 ± 0.170 μm with mancozeb 1 μg/ml ($P < 0.01$). The number of vacuoles doubled in GCs exposed to concentrations of mancozeb higher than

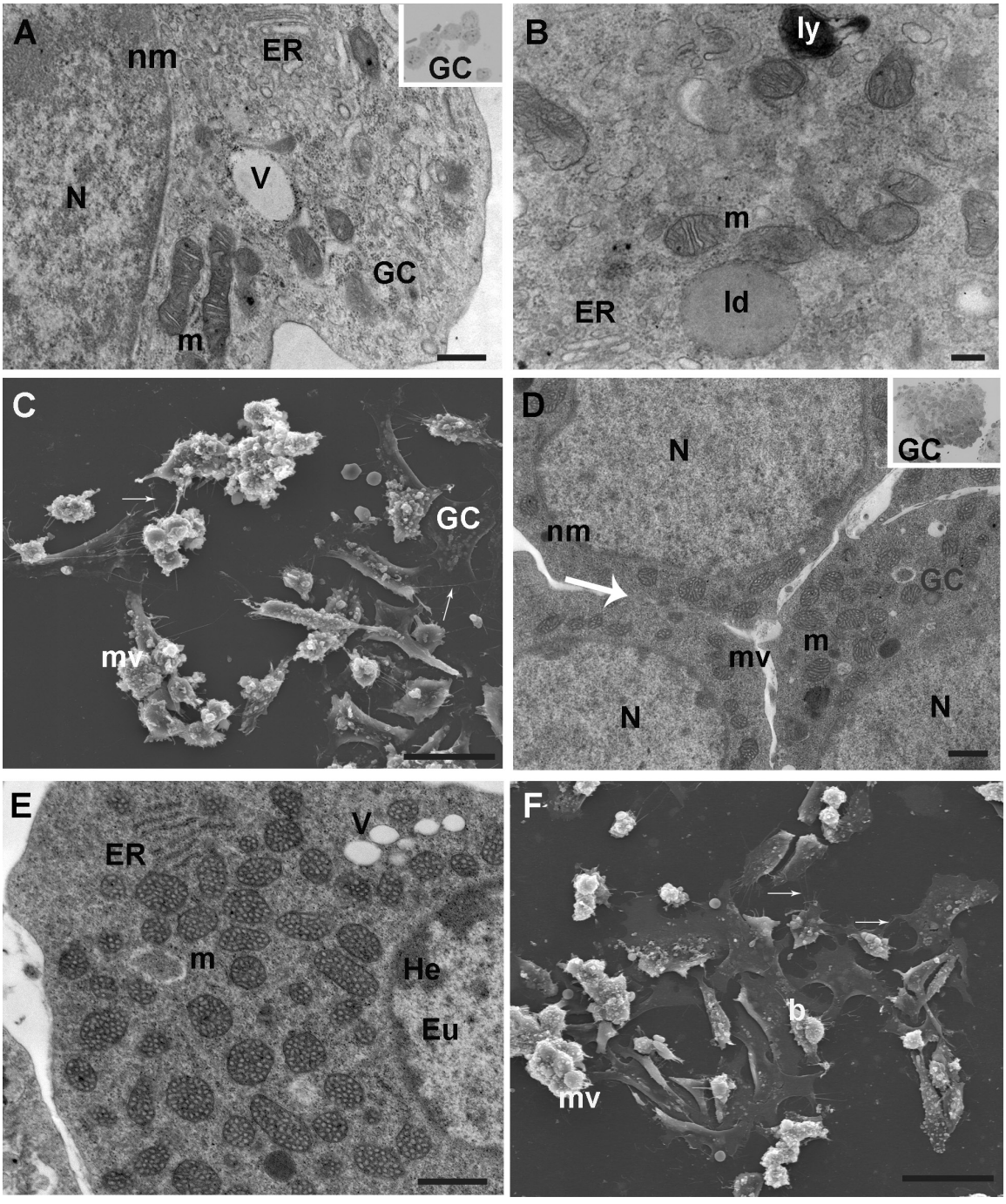

Fig. 1. Ultrastructural analysis of GCs in control and mancozeb 0.001 µg/ml groups. A–C. *Control.* A. Ultrastructure of a granulosa cell (GC) with a large nucleus (N) delimited by a continuous nuclear membrane (nm), numerous round/ovoid mitochondria (m) with extensive cristae, and elements of the endoplasmic reticulum (ER). A vacuole (V) with electron-lucent content is also shown (TEM. Bar: 400 nm). *Inset in A:* A representative image of a semithin section of GCs (LM. Mag: 40 ×). B. Cytoplasmic content of a GC showing a lysosome (Ly), lipid droplets (ld), tubular elements of the endoplasmic reticulum (ER), and mitochondria (m) surrounded by a double membrane (TEM. Bar: 200 nm). C. Adjacent cells (GC) are connected by numerous long, thin pseudopodia (arrows). The surface of the outer layer of GCs shows densely packed microvilli (mv) (SEM. Bar: 40 µm). D–F. *Mancozeb 0.001 µg/ml*. D. Three granulosa cells (GC) with roundish nuclei (N) and small spots of marginalized chromatin under the double layer of the nuclear membrane (nm). Numerous mitochondria (m) and extensive mitochondrial cristae are visible in the cytoplasm. Arrow indicates intercellular connections among adjacent cells; mv: short microvilli (TEM. Bar: 1 µm). *Inset in D.* A representative image of a semithin section of GCs (LM. Mag: 40 ×). E. At high magnification, a transversal section evidences the arrangement of numerous mitochondrial cristae of mitochondria (m) and parallel tubular elements of the endoplasmic reticulum (ER). V: vacuoles; He: heterochromatin; Eu: euchromatin (TEM. Bar: 1 µm). F. Adherent granulosa cells (GCs), with a smooth appearance, are covered by roundish cells covered by numerous microvilli (mv). GCs are connected by means of numerous long, thin pseudopodia (arrows) (SEM. Bar: 40 µm).

Table 1. Summary of main results obtained by TEM and SEM observations –Comparisons of ultrastructural characteristics were performed with respect to the less-exposed group

	Control	Mancozeb			
		0.001 μg/ml	0.01 μg/ml	0.1 μg/ml	1 μg/ml
Nuclear membrane shape	roundish	roundish	invaginated	invaginated	invaginated or interrupted
Chromatin	uniformly distributed; occasionally clustered	uniformly distributed; occasionally condensed and marginalized	condensed and marginalized	condensed and marginalized	condensed and marginalized
Mitochondria	numerous, rich of electron-dense cristae	numerous, rich of electron-dense cristae	numerous, rich of electron-dense cristae	numerous, rich of cristae	less visible, more opalescent and with less electron-dense cristae
Vacuoles	few	few	numerous	numerous	abundant
Cytoplasmic projection	numerous, long and thin	numerous, long and thin	reduced in number and length	reduced in number and length	rare and short
Microvilli	numerous, long and thin	numerous, long and thin	less numerous, shorter and thicker	less numerous, shorter and thicker	rare, short and thick
Blebbing	occasional	occasional	occasional	frequent	numerous
Cell debris/fragments	rare	rare	occasional	frequent	abundant

0.01 μg/ml (~16) compared to that of control and mancozeb 0.01 μg/ml groups (~8) ($P < 0.01$) (Table 2).

Discussion

In this study, we aimed to investigate the effects of mancozeb—a fungicide commonly used for its low toxicity—on cell ultrastructure in a model of reproductive toxicity previously used to study the hexachlorocyclohexane lindane [12], and comprising mouse GCs cultured *in vitro* in the presence or absence of increasing concentrations of mancozeb.

Results obtained by TEM and SEM indicated the harmful action of this fungicide on the somatic compartment of the mouse ovarian follicle, with dose-related effects. The gonadal toxicity of mancozeb has previously been shown *in vivo* to impair fertilization [27], disrupt the estrous cycle, significantly decrease the number of healthy follicles, and increase the number of atretic follicles [28]. Our previous *in vitro* studies in GCs, which used a biomolecular approach, revealed that concentrations of mancozeb ranging from 0.001 to 1 μg/ml induced the reorganization of the actin cytoskeleton, the acquisition of migratory capacity, and a significant decrease in p53 expression levels, without the involvement of caspase proteins 3 and 7, which are activators of apoptosis [10]. Furthermore, GCs exposed to 0.01 μg/ml of mancozeb showed a low p53 content, depolarized mitochondrial membrane potential ($\Delta\Psi m$), low ATP, and reduced glutathione (GSH) levels associated with increased ROS generation [11]. Conversely, embryo toxicity tests revealed that the exposure of mouse embryos to 0.003 μg/ml of mancozeb for 96 h induced apoptosis in blastomeres [29]. This discrepancy can be justified by the longer culture period [29]. It is also possible that rescue mechanisms, likely connected to Akt pathway activation [11, 30], may counteract only the initial harmful effects of the fungicide but not effects attributable to chronic exposure or to higher concentrations of mancozeb.

Therefore, to obtain a detailed morphological description of the status of GCs exposed *in vitro* to increasing concentrations of mancozeb, we used electron microscopy, considered the gold-standard for the determination of cell death and identification of apoptosis [31, 32]. Our morphological analysis of mouse GCs exposed to increasing concentrations of mancozeb evidenced high preservation of both nucleus and cytoplasmic organelles at the lowest concentration. However, presumptive indicators of cell death were observed already at the lowest doses, and ranged from 1) early signs such as chromatin condensation and marginalization under the nuclear membrane (only occasionally seen in GCs treated with 0.001 μg/ml); 2) intermediate signs such as nuclear membrane indentation, vacuolization, and reduction of the microvillar-covered surface; and 3) late signs such as membrane blebbing and the presence of cellular debris. Morphological findings obtained by electron microscopy showed signs of cell death compatible with apoptosis (as previously reviewed [32]), but probably associated with secondary necrosis due to *in vitro* conditions (see the "apoptosis-necrosis continuum" described previously [33] for further details).

Other studies have described ultrastructural changes in apoptotic cells comparable with those found in the present study, such as chromatin marginalization, nuclear alteration, cytoplasmic reorganization, and loss of membrane integrity [34, 35]. Apoptotic GCs showed progressive alterations in the nuclear envelope form, the presence of condensed chromatin around the inner margins of the nuclear membrane, and cytoplasmic vacuolation [36], in accordance with our findings.

However, vacuolization observed at the highest concentrations, both as increased numbers (significantly higher compared with 0.01 μg/ml of mancozeb) and dimension (significantly higher at a concentration as low as 0.001 μg/ml mancozeb) may be the result of autophagic phenomena, with degradative autophagic structures (autolysosomes) encircled by a single membrane and containing partially degraded materials with a high electron density [37]. It is noteworthy that the mitochondrial ultrastructure appeared to

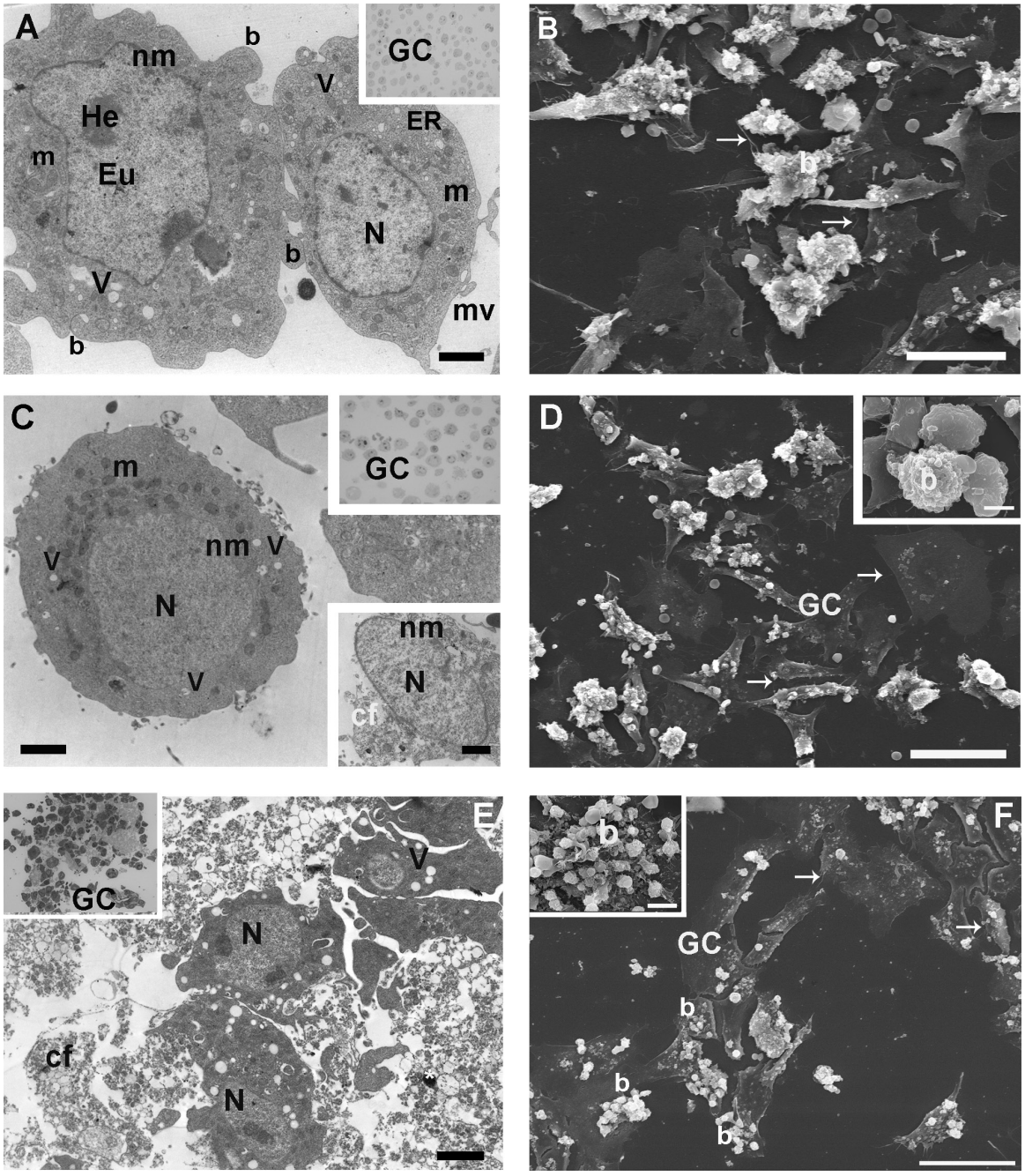

Fig. 2. Ultrastructural analysis of GCs in mancozeb 0.01–1 µg/ml groups. A–B. *Mancozeb 0.01 µg/ml.* A. Two adjacent granulosa cells (GCs) with different phenotypes: the one on the right, with a roundish shape and nucleus (N), shows good preservation of the cytoplasm with numerous mitochondria (m), vacuoles (V), and endoplasmic reticulum (ER); the other on the left, with high preservation of mitochondria (m), vacuoles (V), and other organelles, shows significant blebbing (b). He: heterochromatin; Eu: euchromatin (TEM. Bar: 2 µm). *Inset in A:* Representative image of a semithin section of GCs (LM. Mag: 40 ×). B. Smooth, adherent GCs covered with irregular cells with highly blebbed surfaces (b). Connecting pseudopodia (arrows) are reduced in number and extension (SEM. Bar: 40 µm). C–D. *Mancozeb 0.1 µg/ml*. C. Granulosa cell (GC) showing high preservation with numerous ovoid mitochondria (m), surrounding a nucleus (N) delimited by a nuclear membrane (nm). *Upper inset in C:* Representative image of a semithin section of GCs (LM. Mag: 40 ×). *Lower inset in C:* Altered GCs with cytoplasmic fragments (cf) released in proximity to the nucleus (N); nm: nuclear membrane. D. Smooth adherent GCs are covered by small and roundish blebs; superficial GCs appear rich of blebs. Arrows: detail of pseudopodia, short and rare (SEM. Bar: 40 µm). *Inset in D:* High magnification of a cytoplasmic bleb (b) (SEM. Bar: 8 µm). E–F. *Mancozeb 1 µg/ml*. E. Altered, irregularly-shaped cells, highly vacuolated (V) and with extensive blebbing (b), interspersed in cell fragments (cf), containing numerous membrane-bound organelle remnants, and debris (*) (TEM. Bar: 4 µm). N: nucleus. *Inset in E:* Representative image of a semithin section of GCs (LM, Mag: 40 ×). F. Abundant blebbing (b) is visible on the GC surface. Note the scarcity of cytoplasmic projections (arrow), with a *quasi*-absence of pseudopodia (SEM. Bar: 40 µm). *Inset in F:* High magnification of degenerating GCs, completely covered by cytoplasmic blebs (b) (SEM. Bar: 8 µm).

Table 2. Dimension and number (expressed as mean ± standard deviation) of mitochondria and vacuoles in granulosa cells (GCs) exposed or not (control) to mancozeb 0.001–1 μg/m

	Control	Mancozeb			
		0.001 μg/ml	0.01 μg/ml	0.1 μg/ml	1 μg/ml
Mitochondria (μm)	0.550 ± 0.074 [a]	0.539 ± 0.127 [a]	0.364 ± 0.091 [b]	0.366 ± 0.074 [b]	0.437 ± 0.087 [b]
N. of mitochondria	25 ± 8 [a]	24 ± 8 [a]	29 ± 9 [a]	40 ± 6 [b]	24 ± 11 [a]
Vacuoles (μm)	0.336 ± 0.141 [a]	0.546 ± 0.186 [b]	0.689 ± 0.314 [b]	0.804 ± 0.289 [b, c]	1.059 ± 0.170 [c]
N. of vacuoles	8 ± 4 [a]	9 ± 4 [a]	15 ± 4 [b]	16 ± 5 [b]	16 ± 4 [b]

Approximately 10–20 mitochondria and 5–10 vacuoles were measured in low magnification TEM micrographs from at least 15 GCs from three different experiments. Morphometry was performed using one-way ANOVA with Tukey's HSD post-hoc analysis.

be properly maintained in integral cells, including at the highest concentrations. However, the reduction in mitochondrial size observed in groups treated with mancozeb 0.01–1 μg/ml, associated with the absence of electron-dense cristae and a homogeneous matrix, may be indicative of pre-apoptotic changes [38].

The inhibition of intercellular junctions followed by the disconnection of adjacent cells has been shown to severely disrupt communication between oocytes and GCs, thus inhibiting the supply with consequent GC atresia and loss of oocyte development capacity [39, 40]. Therefore, our findings on the dose-dependent reduction in the microvillar layer, increase in membrane blebbing, and decrease in pseudopodia and intercellular junctions exerted by mancozeb may represent major causes of reduced/delayed/missed oocyte maturation observed in cases of infertility associated with exposure to pesticides such as mancozeb.

The results obtained from this study confirm that mancozeb may be a possible cause of infertility in exposed human populations [3, 4]. Since GCs actively participate in the development and maturation of the oocyte and cooperate with theca cells in the production of steroids [41], alterations in their normal physiological functions may affect the capacity of oocytes to complete meiosis and become fertilized [42]. This observation should consider that endocrine-disrupting pesticides can interfere with the development and maintenance of secondary sexual characters and sexual behaviors. In fact, it has recently been reported that *in vivo* exposure to mancozeb induces a significant reduction in plasma levels of luteinizing hormone (LH) and testosterone, a slight reduction in follicle stimulating hormone (FSH), and an increase in estradiol and prolactin levels [43].

In conclusion, the results of the present study are the first to indicate that mancozeb exerts dose-dependent toxic effects against the ultrastructure of GCs *in vitro*, with associated indications of cell death. Given that the toxic effects of mancozeb are also exerted in oocytes, as previously demonstrated [9], a study on the ultrastructural analysis of exposed cumulus-oocyte complexes is warranted, as these effects have not yet been demonstrated to our knowledge. Moreover, GC alterations may be associated with reduced oocyte and sterility capacity [44], and therefore ultrastructural analysis of oocytes from exposed OCCs may highlight how impairments in somatic compartments can affect oocyte ultrastructure. These results are likely to be of significant interest in the study of fertility preservation, in both animals and humans.

References

1. **López-Fernández O, Yáñez R, Rial-Otero R, Simal-Gándara J.** Kinetic modelling of mancozeb hydrolysis and photolysis to ethylenethiourea and other by-products in water. *Water Res* 2016; **102**: 561–571. [Medline] [CrossRef]
2. **Runkle J, Flocks J, Economos J, Dunlop AL.** A systematic review of Mancozeb as a reproductive and developmental hazard. *Environ Int* 2017; **99**: 29–42. [Medline] [CrossRef]
3. **Iorio R, Castellucci A, Ventriglia G, Teoli F, Cellini V, Macchiarelli G, Cecconi S.** Ovarian toxicity: from environmental exposure to chemotherapy. *Curr Pharm Des* 2014; **20**: 5388–5397. [Medline] [CrossRef]
4. **Cecconi S, Paro R, Rossi G, Macchiarelli G.** The effects of the endocrine disruptors dithiocarbamates on the mammalian ovary with particular regard to mancozeb. *Curr Pharm Des* 2007; **13**: 2989–3004. [Medline] [CrossRef]
5. **Nordby KC, Andersen A, Irgens LM, Kristensen P.** Indicators of mancozeb exposure in relation to thyroid cancer and neural tube defects in farmers families. *Scand J Work Environ Health* 2005; **31**: 89–96. [Medline] [CrossRef]
6. **Mohanty B, Pandey SP, Tsutsui K.** Thyroid disrupting pesticides impair the hypothalamic-pituitary-testicular axis of a wildlife bird, Amandava amandava. *Reprod Toxicol* 2017; **71**: 32–41. [Medline] [CrossRef]
7. **Jacobsen PR, Axelstad M, Boberg J, Isling LK, Christiansen S, Mandrup KR, Berthelsen LO, Vinggaard AM, Hass U.** Persistent developmental toxicity in rat offspring after low dose exposure to a mixture of endocrine disrupting pesticides. *Reprod Toxicol* 2012; **34**: 237–250. [Medline] [CrossRef]
8. **Hass U, Boberg J, Christiansen S, Jacobsen PR, Vinggaard AM, Taxvig C, Poulsen ME, Herrmann SS, Jensen BH, Petersen A, Clemmensen LH, Axelstad M.** Adverse effects on sexual development in rat offspring after low dose exposure to a mixture of endocrine disrupting pesticides. *Reprod Toxicol* 2012; **34**: 261–274. [Medline] [CrossRef]
9. **Rossi G, Palmerini MG, Macchiarelli G, Buccione R, Cecconi S.** Mancozeb adversely affects meiotic spindle organization and fertilization in mouse oocytes. *Reprod Toxicol* 2006; **22**: 51–55. [Medline] [CrossRef]
10. **Paro R, Tiboni GM, Buccione R, Rossi G, Cellini V, Canipari R, Cecconi S.** The fungicide mancozeb induces toxic effects on mammalian granulosa cells. *Toxicol Appl Pharmacol* 2012; **260**: 155–161. [Medline] [CrossRef]
11. **Iorio R, Castellucci A, Rossi G, Cinque B, Cifone MG, Macchiarelli G, Cecconi S.** Mancozeb affects mitochondrial activity, redox status and ATP production in mouse granulosa cells. *Toxicol In Vitro* 2015; **30**(1 Pt B): 438–445. [Medline] [CrossRef]
12. **Palmerini MG, Zhurabekova G, Balmagambetova A, Nottola SA, Miglietta S, Belli M, Bianchi S, Cecconi S, Di Nisio V, Familiari G, Macchiarelli G.** The pesticide Lindane induces dose-dependent damage to granulosa cells in an in vitro culture. *Reprod Biol* 2017; S1642-431X(17)30148-1. (in press). [Medline]
13. **Khalili MA, Shahedi A, Ashourzadeh S, Nottola SA, Macchiarelli G, Palmerini MG.** Vitrification of human immature oocytes before and after in vitro maturation: a review. *J Assist Reprod Genet* 2017; **34**: 1413–1426. [Medline] [CrossRef]
14. **Coticchio G, Dal Canto M, Fadini R, Mignini Renzini M, Guglielmo MC, Miglietta S, Palmerini MG, Macchiarelli G, Nottola SA.** Ultrastructure of human oocytes after in vitro maturation. *Mol Hum Reprod* 2016; **22**: 110–118. [Medline] [CrossRef]
15. **Leoni GG, Palmerini MG, Satta V, Succu S, Pasciu V, Zinellu A, Carru C, Macchiarelli G, Nottola SA, Naitana S, Berlinguer F.** Differences in the kinetic of the first meiotic division and in active mitochondrial distribution between prepubertal and adult oocytes mirror differences in their developmental competence in a sheep model. *PLoS ONE* 2015; **10**: e0124911. [Medline] [CrossRef]
16. **Palmerini MG, Nottola SA, Leoni GG, Succu S, Borshi X, Berlinguer F, Naitana S, Bekmukhambetov Y, Macchiarelli G.** In vitro maturation is slowed in prepubertal lamb oocytes: ultrastructural evidences. *Reprod Biol Endocrinol* 2014; **12**: 115. [Medline] [CrossRef]

17. **Palmerini MG, Antinori M, Maione M, Cerusico F, Versaci C, Nottola SA, Macchiarelli G, Khalili MA, Antinori S.** Ultrastructure of immature and mature human oocytes after cryotop vitrification. *J Reprod Dev* 2014; **60**: 411–420. [Medline] [CrossRef]
18. **Khalili MA, Maione M, Palmerini MG, Bianchi S, Macchiarelli G, Nottola SA.** Ultrastructure of human mature oocytes after vitrification. *Eur J Histochem* 2012; **56**: e38. [Medline] [CrossRef]
19. **Nottola SA, Heyn R, Camboni A, Correr S, Macchiarelli G.** Ultrastructural characteristics of human granulosa cells in a coculture system for in vitro fertilization. *Microsc Res Tech* 2006; **69**: 508–516. [Medline] [CrossRef]
20. **Nottola SA, Albani E, Coticchio G, Palmerini MG, Lorenzo C, Scaravelli G, Borini A, Levi-Setti PE, Macchiarelli G.** Freeze/thaw stress induces organelle remodeling and membrane recycling in cryopreserved human mature oocytes. *J Assist Reprod Genet* 2016; **33**: 1559–1570. [Medline] [CrossRef]
21. **Palmerini MG, Nottola SA, Tunjung WA, Kadowaki A, Bianchi S, Cecconi S, Sato E, Macchiarelli G.** EGF-FSH supplementation reduces apoptosis of pig granulosa cells in co-culture with cumulus-oocyte complexes. *Biochem Biophys Res Commun* 2016; **481**: 159–164. [Medline] [CrossRef]
22. **Macchiarelli G, Palmerini MG, Nottola SA, Cecconi S, Tanemura K, Sato E.** Restoration of corpus luteum angiogenesis in immature hypothyroid rdw rats after thyroxine treatment: morphologic and molecular evidence. *Theriogenology* 2013; **79**: 116–126. [Medline] [CrossRef]
23. **Macchiarelli G, Nottola SA, Palmerini MG, Bianchi S, Maione M, Lorenzo C, Stifano G, Di Marco E, Correr S.** Morphological expression of angiogenesis in the mammalian ovary as seen by SEM of corrosion casts. *Ital J Anat Embryol* 2010; **115**: 109–114. [Medline]
24. **Martelli A, Palmerini MG, Russo V, Rinaldi C, Bernabò N, Di Giacinto O, Berardinelli P, Nottola SA, Macchiarelli G, Barboni B.** Blood vessel remodeling in pig ovarian follicles during the periovulatory period: an immunohistochemistry and SEM-corrosion casting study. *Reprod Biol Endocrinol* 2009; **7**: 72. [Medline] [CrossRef]
25. **Nottola SA, Makabe S, Stallone T, Familiari G, Correr S, Macchiarelli G.** Surface morphology of the zona pellucida surrounding human blastocysts obtained after in vitro fertilization. *Arch Histol Cytol* 2005; **68**: 133–141. [Medline] [CrossRef]
26. **DErcole S, Tripodi D, Marzo G, Bernardi S, Continenza MA, Piattelli A, Iaculli F, Mummolo S.** Microleakage of bacteria in different implant-abutment assemblies: an in vitro study. *J Appl Biomater Funct Mater* 2015; **13**: e174–e180. [Medline]
27. **Rossi G, Buccione R, Baldassarre M, Macchiarelli G, Palmerini MG, Cecconi S.** Mancozeb exposure in vivo impairs mouse oocyte fertilizability. *Reprod Toxicol* 2006; **21**: 216–219. [Medline] [CrossRef]
28. **Baligar PN, Kaliwal BB.** Induction of gonadal toxicity to female rats after chronic exposure to mancozeb. *Ind Health* 2001; **39**: 235–243. [Medline] [CrossRef]
29. **Greenlee AR, Ellis TM, Berg RL.** Low-dose agrochemicals and lawn-care pesticides induce developmental toxicity in murine preimplantation embryos. *Environ Health Perspect* 2004; **112**: 703–709. [Medline] [CrossRef]
30. **Cecconi S, Rossi G, Santilli A, Stefano LD, Hoshino Y, Sato E, Palmerini MG, Macchiarelli G.** Akt expression in mouse oocytes matured in vivo and in vitro. *Reprod Biomed Online* 2010; **20**: 35–41. [Medline] [CrossRef]
31. **Pandey SP, Tsutsui K, Mohanty B.** Endocrine disrupting pesticides impair the neuroendocrine regulation of reproductive behaviors and secondary sexual characters of red munia (Amandava amandava). *Physiol Behav* 2017; **173**: 15–22. [Medline] [CrossRef]
32. **White MK, Cinti C.** A morphologic approach to detect apoptosis based on electron microscopy. *Methods Mol Biol* 2004; **285**: 105–111. [Medline]
33. **Zeiss CJ.** The apoptosis-necrosis continuum: insights from genetically altered mice. *Vet Pathol* 2003; **40**: 481–495. [Medline] [CrossRef]
34. **Burattini S, Falcieri E.** Analysis of cell death by electron microscopy. *Methods Mol Biol* 2013; **1004**: 77–89. [Medline] [CrossRef]
35. **Elmore S.** Apoptosis: a review of programmed cell death. *Toxicol Pathol* 2007; **35**: 495–516. [Medline] [CrossRef]
36. **Bhardwaj JK, Saraf P.** Transmission electron microscopic analysis of malathion-induced cytotoxicity in granulosa cells of caprine antral follicles. *Ultrastruct Pathol* 2016; **40**: 43–50. [Medline] [CrossRef]
37. **Uchiyama Y, Shibata M, Koike M, Yoshimura K, Sasaki M.** Autophagy-physiology and pathophysiology. *Histochem Cell Biol* 2008; **129**: 407–420. [Medline] [CrossRef]
38. **Cheville NF.** In: Ultrastructural Pathology: The Comparative Cellular Basis of Disease, Second Edition. June 2009, Wiley-Blackwell.
39. **Motta PM, Nottola SA, Pereda J, Croxatto HB, Familiari G.** Ultrastructure of human cumulus oophorus: a transmission electron microscopic study on oviductal oocytes and fertilized eggs. *Hum Reprod* 1995; **10**: 2361–2367. [Medline] [CrossRef]
40. **Hutt KJ, Albertini DF.** An oocentric view of folliculogenesis and embryogenesis. *Reprod Biomed Online* 2007; **14**: 758–764. [Medline] [CrossRef]
41. **Canipari R, Cellini V, Cecconi S.** The ovary feels fine when paracrine and autocrine networks cooperate with gonadotropins in the regulation of folliculogenesis. *Curr Pharm Des* 2012; **18**: 245–255. [Medline] [CrossRef]
42. **Dumesic DA, Meldrum DR, Katz-Jaffe MG, Krisher RL, Schoolcraft WB.** Oocyte environment: follicular fluid and cumulus cells are critical for oocyte health. *Fertil Steril* 2015; **103**: 303–316. [Medline] [CrossRef]
43. **Kjeldsen LS, Ghisari M, Bonefeld-Jørgensen EC.** Currently used pesticides and their mixtures affect the function of sex hormone receptors and aromatase enzyme activity. *Toxicol Appl Pharmacol* 2013; **272**: 453–464. [Medline] [CrossRef]
44. **Kidder GM, Vanderhyden BC.** Bidirectional communication between oocytes and follicle cells: ensuring oocyte developmental competence. *Can J Physiol Pharmacol* 2010; **88**: 399–413. [Medline] [CrossRef]